Importin-α-Mediated Nucleolar Localization of Potato Mop-Top Virus TRIPLE GENE BLOCK1 (TGB1) Protein Facilitates Virus Systemic Movement, Whereas TGB1 Self-Interaction Is Required for Cell-to-Cell Movement in *Nicotiana benthamiana*[1][OPEN]

Nina I. Lukhovitskaya, Graham H. Cowan, Ramesh R. Vetukuri, Jens Tilsner, Lesley Torrance, and Eugene I. Savenkov*

Department of Plant Biology, Uppsala BioCenter, Linnean Centre of Plant Biology, Swedish University of Agricultural Sciences, 75007 Uppsala, Sweden (N.I.L., R.R.V., E.I.S.); Cell and Molecular Sciences, The James Hutton Institute, Dundee DD2 5DA, United Kingdom (G.H.C., J.T., L.T.); and Biomedical Sciences Research Complex, University of St. Andrews, Fife KY16 9ST, United Kingdom (J.T., L.T.)

ORCID ID: 0000-0002-5802-5089 (E.I.S.).

Recently, it has become evident that nucleolar passage of movement proteins occurs commonly in a number of plant RNA viruses that replicate in the cytoplasm. Systemic movement of *Potato mop-top virus* (PMTV) involves two viral transport forms represented by a complex of viral RNA and TRIPLE GENE BLOCK1 (TGB1) movement protein and by polar virions that contain the minor coat protein and TGB1 attached to one extremity. The integrity of polar virions ensures the efficient movement of RNA-CP, which encodes the virus coat protein. Here, we report the involvement of nuclear transport receptors belonging to the importin-α family in nucleolar accumulation of the PMTV TGB1 protein and, subsequently, in the systemic movement of the virus. Virus-induced gene silencing of two importin-α paralogs in *Nicotiana benthamiana* resulted in significant reduction of TGB1 accumulation in the nucleus, decreasing the accumulation of the virus progeny in upper leaves and the loss of systemic movement of RNA-CP. PMTV TGB1 interacted with importin-α in *N. benthamiana*, which was detected by bimolecular fluorescence complementation in the nucleoplasm and nucleolus. The interaction was mediated by two nucleolar localization signals identified by bioinformatics and mutagenesis in the TGB1 amino-terminal domain. Our results showed that while TGB1 self-interaction is needed for cell-to-cell movement, importin-α-mediated nucleolar targeting of TGB1 is an essential step in establishing the efficient systemic infection of the entire plant. These results enabled the identification of two separate domains in TGB1: an internal domain required for TGB1 self-interaction and cell-to-cell movement and the amino-terminal domain required for importin-α interaction in plants, nucleolar targeting, and long-distance movement.

Pomoviruses are causal agents of important diseases affecting potato (*Solanum tuberosum*), sugar beet (*Beta vulgaris*), and bean (*Phaseolus vulgaris*). *Potato mop-top virus* (PMTV), the type member of the genus *Pomovirus*, causes an economically important disease of potato called spraing, inducing brown lines and arcs internally and on the surface of tubers. PMTV is transmitted by the root- and tuber-infecting plasmodiophorid *Spongospora subterranea* (Jones and Harrison, 1969; Arif et al., 1995).

The pomovirus genome is divided into three single-stranded RNA (ssRNA) segments of positive polarity. RNA-Rep encodes the putative RNA-dependent RNA polymerase, the replicase of the virus (Savenkov et al., 1999). RNA-CP encodes a coat protein (CP) and another protein called CP-RT or minor CP, which is produced by translational read-through of the CP stop codon (Sandgren et al., 2001). Whereas CP is the major structural protein of the virions, CP-RT is incorporated in one of the termini of the virus particles and a domain within the read-through region of the protein is needed for transmission of the virus by its vector (Reavy et al., 1998). Moreover, CP-RT, but not CP, interacts with the major movement protein TRIPLE GENE BLOCK1 (TGB1; Torrance et al., 2009), which is encoded by RNA-TGB. Besides encoding a triple gene block of movement proteins, TGB1, TGB2, and TGB3 (Zamyatnin et al., 2004), RNA-TGB also encodes a viral suppressor of RNA silencing, the 8K protein (Lukhovitskaya et al., 2013b).

[1] This work was supported by the Swedish Research Council Formas (to E.I.S.), the Carl Tryggers Foundation (to E.I.S. and N.I.L.), the Swedish Institute (to N.I.L.), and the Rural and Environmental Science and Analytical Services Division strategic research fund of the Scottish Government (to L.T., J.T., and G.H.C.).

* Address correspondence to eugene.savenkov@slu.se.

The author responsible for distribution of materials integral to the findings presented in this article in accordance with the policy described in the Instructions for Authors (www.plantphysiol.org) is: Eugene I. Savenkov (eugene.savenkov@slu.se).

[OPEN] Articles can be viewed without a subscription.

www.plantphysiol.org/cgi/doi/10.1104/pp.114.254938

To establish a successful infection in the entire plant, viruses must be able to replicate and to move their genomic components between cells, tissues, and organs. Recently, it has become evident that PMTV utilizes a sophisticated mode of cell-to-cell and long-distance movement that involves two virus transport forms, one represented by the viral nucleoprotein complexes (vRNPs) consisting of virus RNA and the TGB1 protein and another represented by the polar virions containing CP-RT and TGB1 proteins attached to one extremity of virus particles (Torrance et al., 2009; for review, see Solovyev and Savenkov, 2014). Proteins implicated in PMTV cell-to-cell movement include TGB1, TGB2, and TGB3 (Zamyatnin et al., 2004; Haupt et al., 2005a). Indirect evidence suggests that CP-RT is required for the efficient systemic movement of intact virions through its interaction with TGB1 (Torrance et al., 2009).

Early in infection, the vRNP is transported on the endoplasmic reticulum actomyosin network and targeted to plasmodesmata by TGB2 and TGB3. Later in infection, fluorescently labeled TGB1 is seen in the nucleus and accumulates in the nucleolus. Nucleolar TGB1 association has been shown to be necessary for long-distance movement (Wright et al., 2010).

Two structurally distinct subdomains have been identified in the N terminus of TGB1 proteins of hordeiviruses and pomoviruses (Makarov et al., 2009), an N-terminal domain (NTD) comprising approximately 125 amino acids in PMTV (Table I) and an internal domain. These domains display sequence-nonspecific binding of ssRNA in noncooperative and cooperative manners, respectively. The C-terminal half of TGB1 contains a nucleoside triphosphatase/helicase domain that displays cooperative RNA binding. Previously, Wright et al. (2010) reported that TGB1 expressed from a 35S promoter localizes in the cytoplasm and accumulates in the nucleus and nucleolus with occasional labeling of microtubules (MTs). The MT labeling was apparent behind the leading edge of infection when yellow fluorescent protein (YFP)-TGB1 was expressed from an infectious clone. Deletion of 84 amino acids from the N terminus of TGB1 (representing most of the NTD) resulted in the absence of MTs, and nucleolar labeling and fusion of these 84 N-terminal amino acids to GFP resulted in nucleolar enrichment of GFP but no labeling of MTs. Deletion of the 5′ proximal part of the TGB1 open reading frame (ORF), encoding this N-terminal 84 amino acids, in the virus clone abolished systemic but not cell-to-cell movement. However, such deletion had no effect on TGB1 interactions with the CP-RT or self-interaction (Wright et al., 2010).

To better understand the function of TGB1 in PMTV infection, including cell-to-cell movement and targeting the nucleolus, which, in turn, is required for efficient systemic movement, we mapped the TGB1 domains needed for virus cell-to-cell movement, identified nucleolar localization signals (NoLSs) within the NTD, and, using bimolecular fluorescence complementation (BiFC), found that TGB1 was associated with importin-α in the nucleus and nucleolus. TGB1 accumulation in the nucleus, virus accumulation in upper leaves, and virus systemic movement were reduced in *Nicotiana benthamiana* plants silenced for importin-α. Together, these results suggest that the importin-α-dependent nucleolar association of TGB1 is required for efficient infection by PMTV.

RESULTS

The N-Terminal Segment of PMTV TGB1 Is Needed for Self-Interaction and Cell-to-Cell Movement

To more precisely define the role of the N terminus of PMTV TGB1 in virus movement and to discriminate between the requirements for PMTV cell-to-cell and long-distance movement, a series of 5′ proximal deletions were engineered into the TGB1 ORF of the infectious clone (Savenkov et al., 2003). The deletions resulted in N-terminal truncations of TGB1 with an interval of 20 to 80 amino acids spanning a 747-nucleotide-long 5′ proximal region of the TGB1 ORF and were designated as Δ44 (44-amino acid truncation from the N terminus), Δ84 (published previously by Wright et al. [2010]), Δ149, Δ169, and Δ249 (Fig. 1). Notably, the longest truncation analyzed (Δ249 mutant) spans not only the N-terminal and internal domains but also includes part of the helicase domain of TGB1. In vitro-generated transcripts for each of the mutants along with RNA-Rep and RNA-CP

Table I. *Structural features of the PMTV TGB1 protein*

Positively charged amino acids are set in boldface type and underscored. NoD, Nucleolar localization sequence detector; NS, not shown.

TGB1 Sequence	Sequence Location	Predicted Features	Algorithm
NS	1 to 125	Unstructured/disordered domain (NTD)	PDISORDER, IUPred, RONN
H**R**V**KK**D	11 to 16	NoLSA	NoD
F**R**TNNN**KK**TQNW**K**P**R**S	37 to 52	NoLSB	NoD
NS	126 to 180	Ordered domain (internal domain)	PDISORDER, Phyre 2
AEFFKSSGLLEKFDFYLSSR	161 to 180	α-Helix	PSS Finder, Phyre 2
NS	211 to 436	Viral superfamily 1 RNA helicases	National Center for Biotechnology Information database
NS	211 to 229	P-loop-containing nucleoside triphosphatase	National Center for Biotechnology Information database

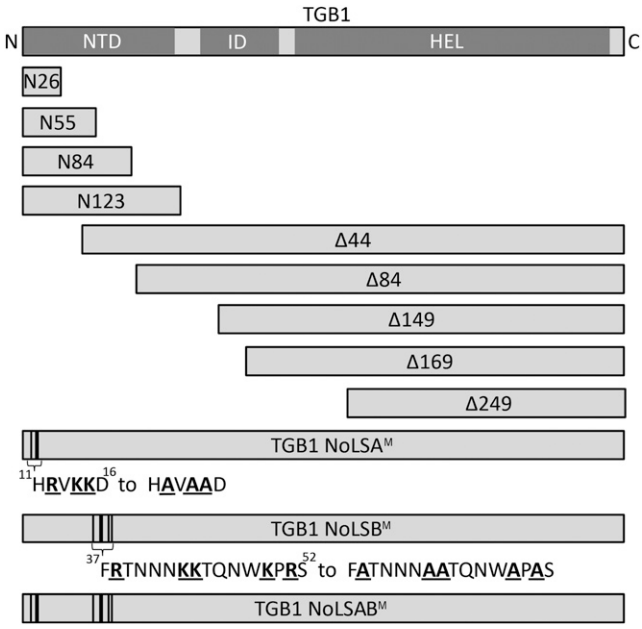

Figure 1. Schematic representation of the TGB1 constructs used in this study. Schematics are shown for full-length TGB1, N-terminal truncations (Δ), N-terminal fragments (N), and amino acid substitutions in the NoLS of PMTV TGB1 analyzed in this article. At top is the domain structure of the PMTV TGB1 protein. The N-terminal fragments and N-terminal truncations are shown to scale. Superscript numbers refer to amino acid residue positions within the sequence of the TGB1 protein. ID, Internal domain; HEL, helicase domain.

transcripts were inoculated on *N. benthamiana* plants. At 14 d post inoculation (dpi), the inoculated and upper noninoculated leaves were analyzed by ELISA, northern blot, and reverse transcription (RT)-PCR. The three methods showed consistent results demonstrating that Δ44, Δ84, and Δ149 (but not Δ169 and Δ249) were readily detectable in the inoculated leaves, indicative of efficient cell-to-cell movement (Fig. 2, A and B; Supplemental Fig. S1A), and Δ44 (but not Δ149, Δ169, and Δ249) was also detectable in upper leaves, indicative of systemic movement (Fig. 2A; Table II; Supplemental Fig. S1, B and C). Δ84 showed an intermediate phenotype in terms of systemic movement. Previous experiments based only on detection by northern blot and ELISA indicated that Δ84 was unable to move to upper leaves (Wright et al., 2010), and that was confirmed in this study as accumulation of the virus in upper leaves was below detection limits by ELISA (Fig. 2A; Supplemental Fig. S1B). However, RT-PCR, a detection method more sensitive than northern blotting or ELISA, detected RNA-TGB.Δ84 (in four out of 10 plants in two experiments) and RNA-CP (in two out of 10 plants in two experiments) in the upper leaves (Supplemental Fig. S1C). Thus, Δ84 moves long distance only very inefficiently, and longer N-terminal truncations of the TGB1 protein abolish systemic movement altogether.

Since PMTV moves in two forms, as a vRNP complex consisting of viral RNA and TGB1 and as virus particles, and PMTV TGB1 was shown previously to self-interact (Torrance et al., 2009), we hypothesized that oligomerization (self-interaction) of the TGB1 protein might be needed for efficient formation of cell-to-cell movement-competent vRNPs. To address this question, we studied the self-interactions of the truncated TGB1 proteins using the yeast two-hybrid and BiFC systems. The yeast (*Saccharomyces cerevisiae*) two-hybrid experiments revealed that Δ44, Δ84, and Δ149 self-interacted, while Δ169 and Δ249 did not (Fig. 2C, blue colonies in diagonal lines at 2 and 16 h of incubation in –UHLW). Similar to the results reported previously, CP-RT/TGB1 interactions (and interactions with the truncated TGB1 variants in this study, respectively) were only detected when TGB1 or its truncated variants were fused to an activation domain and CP-RT to a DNA binding domain (Fig. 2C, white and light blue colonies in horizontal lines at 2 and 16 h of incubation on –UHLW; Torrance et al., 2009), but not in the reciprocal combinations when TGB1 formed a translational fusion with the DNA-binding domain and CP-RT with the activation domain (Fig. 2C; Torrance et al., 2009). This might be due to steric hindrance caused by the 89-kD RT domain. All truncated derivatives of TGB1 retained the ability to bind CP-RT.

Similar results were obtained using BiFC. When Δ84 was fused to the C-terminal half of YFP (Δ84-FP) and TGB1 was fused to the N-terminal half of YFP (Y-TGB1) and transiently coexpressed in epidermal cells by agroinfiltration, reconstituted YFP fluorescence was found on microtubule-like strands and accumulated in the nucleolus (Fig. 2D; Table II). However, these localizations were due to full-length TGB1, as cells coexpressing Y-Δ84 and Δ84-FP showed BiFC signal indicating self-interactions of the truncated protein, but fluorescence was observed only in the cytoplasm and in the nucleus, with no microtubule or nucleolar localization recorded (Fig. 2D; Table II). Similarly, BiFC detected self-interaction of Δ149 without nucleolar localization, but cells coexpressing Y-Δ169 and Δ169-FP yielded no fluorescent signal, indicating that this truncated protein was no longer able to self-interact (Table II; Supplemental Fig. S1D). Expression of Δ84-FP alone, Δ149-FP alone, Δ169-FP alone, or any of these constructs with Y-GST (for glutathione *S*-transferase) served as negative controls. No YFP fluorescence was detected in any of these agroinfiltrations (Supplemental Fig. S1D).

Therefore, the data showed that cell-to-cell movement of the *TGB1* mutants, which express truncated versions of the TGB1 protein, correlated with the ability of the TGB1 variants to oligomerize (self-interact; Fig. 2E), and deletions as long as 447 nucleotides in the TGB1 gene (truncation of 149 amino acids from the TGB1 N terminus) can be tolerated by the virus without any obvious reduction of cell-to-cell movement. On the other hand, efficient long-distance movement requires the presence of a longer NTD, as truncations of 44 to 84 amino acids from the N terminus resulted in impaired, inefficient long-distance movement of the virus and deletion of 149 amino acids from the N terminus abolished

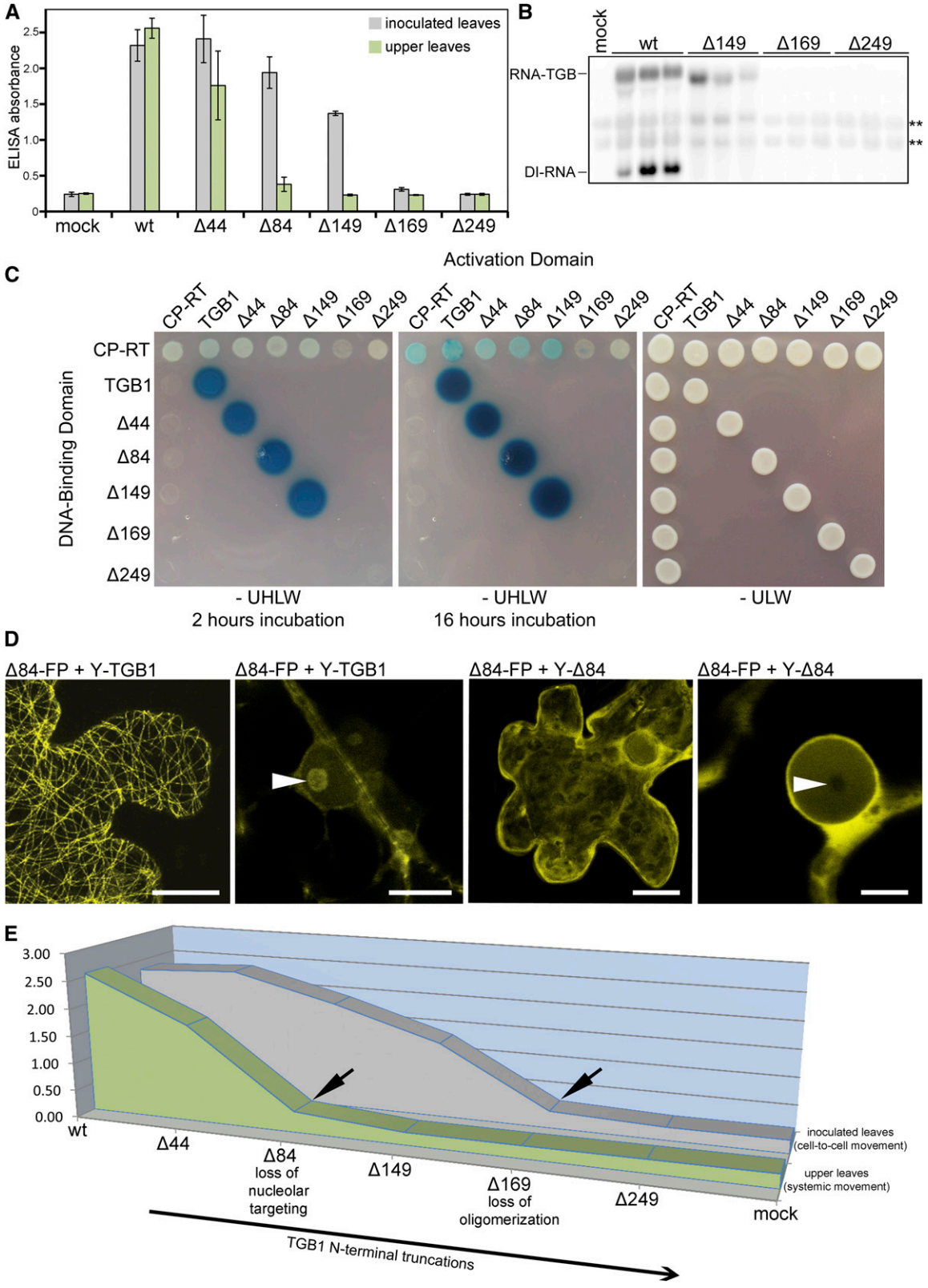

Figure 2. Effects of N-terminal truncations in the PMTV TGB1 protein on viral RNA cell-to-cell and long-distance movement and self-interaction of TGB1. A, Detection of PMTV by ELISA as presented by absorbance values at 405 nm. Plant extracts were prepared from inoculated and upper leaves 14 dpi. The average absorbance of a healthy plant extract was equal to 0.25. The data are from two independent experiments (n = 10); error bars denote SD. B, RNA gel-blot analyses of the accumulation of

Table II. *The PMTV movement phenotypes associated with deletions in the TGB1 gene*
NT, Not tested.

Construct	Cell-to-Cell Movement	Systemic Movement[a]	Yeast Two-Hybrid System Self-Interaction	BiFC Self-Interaction		
				Microtubules (Cytoplasm)	Nucleus	Nucleolus
TGB1 wild type	+	+	+	+	+	+
Δ44	+	+	+	NT	NT	NT
Δ84	+	+[b]	+	+	+	−
Δ149	+	−	+	+	+	−
Δ169	−	−	−	−	−	−
Δ249	−	−	−	NT	NT	NT

[a]As assessed by ELISA, RT-PCR, and northern blot. [b]Weak limited movement.

systemic movement (Fig. 2E; Table II), regardless of the fact that all truncated TGB1 variants interacted with CP-RT, albeit with different efficiency (Fig. 2C). Since the NTD of TGB1 seems to contain NoLS and enters the nucleolus, which, in turn, is needed for virus long-distance movement (Wright at al., 2010), we next analyzed the requirements for nucleolar targeting.

Mapping the Nucleolar Targeting Signal

Our previous results suggested that the N-terminal 84 amino acids of TGB1 contain a nucleolar targeting signal (Wright et al., 2010). In this study, using the nucleolar localization sequence detector algorithm (Scott et al., 2011) and manual inspection of the TGB1 sequence, two putative NoLS motifs were predicted in the N terminus (NoLSA and NoLSB; Table I; Fig. 1), so we compared the localization of TGB1 N-terminal fragments of 26, 55, 84, and 123 amino acids fused to GFP and expressed from a 35S promoter. These experiments revealed that N26-GFP (which contains NoLSA) was partially excluded from the nucleolus (Fig. 3A), whereas N55-GFP and N84-GFP (containing NoLSA and NoLSB) showed strong nucleolar localization (Fig. 3A), and the nucleolar signal was weak for N123-GFP (Fig. 3A). Unfused GFP served as a negative control and was entirely excluded from the nucleolus (Fig. 3A, right). GFP fluorescence of the TGB1 N-terminal fragments was quantified in the nucleus and nucleolus, and the nucleolar-nuclear ratios were compared by ANOVA (Fig. 3C). The quantification confirmed the visual observation and showed that nucleolar accumulation was significantly stronger in N55-GFP and N84-GFP (nucleolar:nuclear ratios of 2.04 and 1.36, respectively) compared with N26-GFP and N123-GFP (nucleolar:nuclear ratios of 0.56 and 0.44, respectively; Fig. 3C), but all TGB1 fragment-GFP fusions analyzed showed increased nucleolar fluorescence compared with unfused GFP (ratio of 0.22). Nucleolar accumulation of N55-GFP was confirmed by colocalization with transiently expressed, monomeric red fluorescent protein (mRFP)-labeled Arabidopsis (*Arabidopsis thaliana*) fibrillarin2 (mRFP-Fib), a marker for nucleoli and Cajal bodies (Fig. 3B; Barneche et al., 2000).

Since N55-GFP showed strong nucleolar localization, this construct was used as a backbone for site-directed mutagenesis of the two putative NoLS to determine if TGB1 amino acid residues 11 to 16 and 37 to 52 were, in fact, NoLS (Fig. 1). Six point mutations were engineered into the N55-GFP expression construct, which resulted in the substitution of three positively charged amino acids with Ala residues in NoLSA (Fig. 1). To abolish NoLSB, 10 point mutations were made, which resulted in the substitution of five positively charged amino acids with Ala residues (Fig. 1; Table I). The mutant N55NoLSA^{M}-GFP and N55NoLSB^{M}-GFP translational

Figure 2. (*Continued.*)
wild-type PMTV (wt) and the PMTV *TGB1* mutants in inoculated leaves of *N. benthamiana*. Total RNA was isolated 14 dpi. RNA-TGB was detected using ^{32}P-labled 5′ untranslated region antisense RNA probe. Asterisks indicate nonspecific binding of the probe. C, Yeast two-hybrid assay for studying self-interactions and CP-RT interactions of TGB1 and its N terminally truncated forms. Wild-type TGB1 or the TGB1 N-terminal truncated sequences were fused to the LexA-DNA-binding domain or the herpes simplex virus protein16 (VP16) transcription activation domain. Transformants were selected for protein interactions on medium lacking uracil, His, Leu, and Trp (–UHLW), a triple dropout medium. Medium lacking uracil, Leu, and Trp (–ULW), a double dropout medium, selected for the input plasmids only and shows growth of the colonies carrying both plasmids as a positive control. As reported previously (Wright et al., 2010), interaction between TGB1 variants and CP-RT could only be detected when CP-RT was fused to the DNA-binding domain and TGB1 to the activation domain (horizontal row at top) but not in the reverse orientation (vertical row at left), possibly due to steric hindrance. β-Galactosidase activity was assessed by agarose overlay assays at two time points (at 2 and 16 h of incubation at 28°C). D, Interaction of full-length TGB1 and Δ84, and self-interaction of Δ84, detected by BiFC. Interacting TGB1 and Δ84 decorate MTs and localize to the nucleolus (arrowhead), whereas self-interacting Δ84 does not localize to MTs, resides mostly in the cytoplasm, and is excluded from the nucleolus (arrowhead). Bars = 10 μm (first three images from left) and 5 μm (fourth image). E, Three-dimensional chart showing the correlation between TGB1 oligomerization, nucleolar targeting, and virus accumulation in inoculated (due to cell-to-cell movement) and upper (due to systemic movement) leaves.

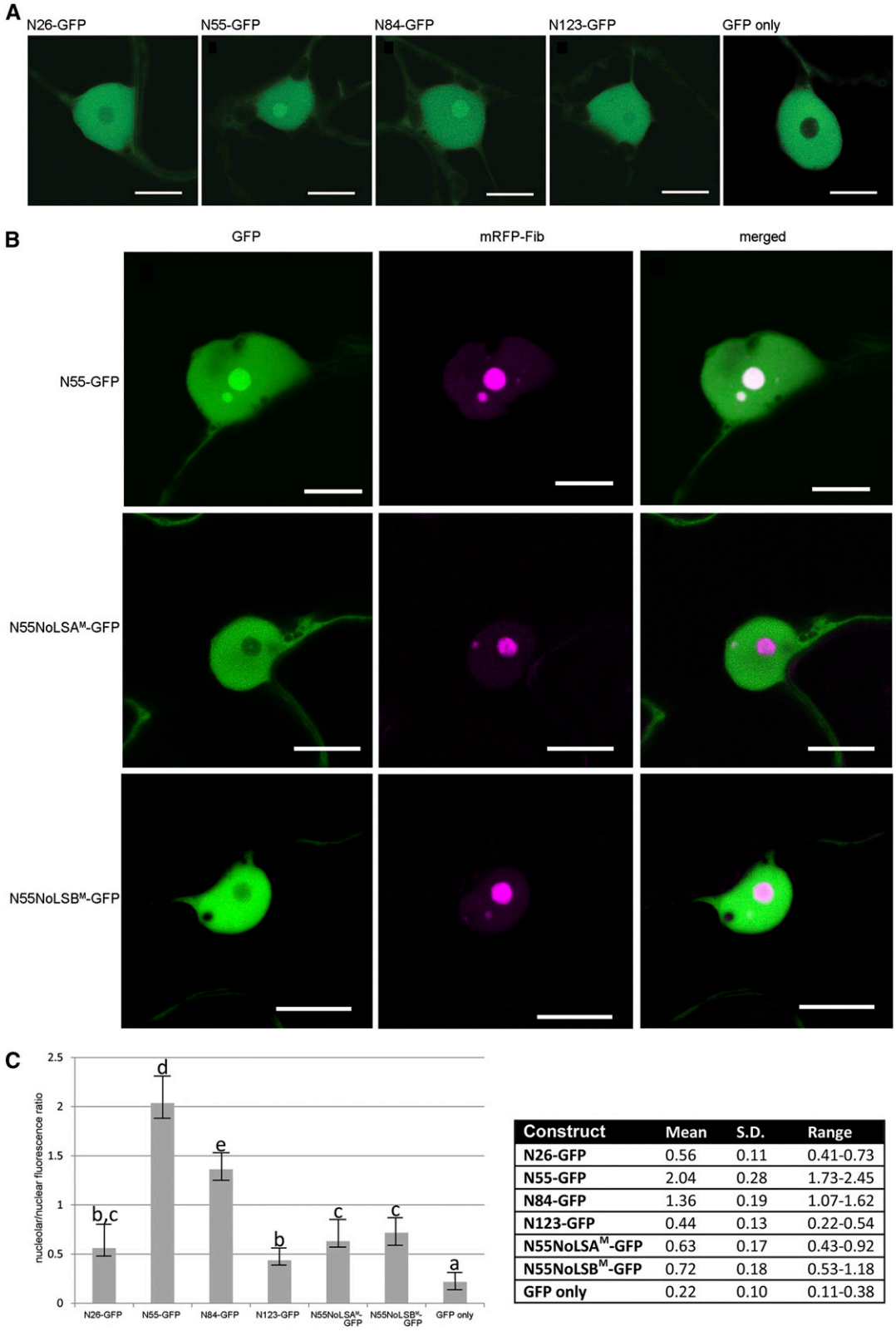

Construct	Mean	S.D.	Range
N26-GFP	0.56	0.11	0.41-0.73
N55-GFP	2.04	0.28	1.73-2.45
N84-GFP	1.36	0.19	1.07-1.62
N123-GFP	0.44	0.13	0.22-0.54
N55NoLSA^{M}-GFP	0.63	0.17	0.43-0.92
N55NoLSB^{M}-GFP	0.72	0.18	0.53-1.18
GFP only	0.22	0.10	0.11-0.38

Figure 3. Nuclear localization of TGB1 N-terminal fragments fused to GFP. A, Accumulation of TGB1 N-terminal fragments (26, 55, 84, and 123 amino acid residues) fused to GFP in the nucleus and their partial exclusion from the nucleolus (N26-GFP and N123-GFP). N55-GFP and N84-GFP accumulate in the nucleoplasm and are enriched within the nucleolus. Bars = 5 μm. B, TGB1 N55-GFP fusion and its two derivatives with amino acids substitutions in the NoLSA and NoLSB motifs (N55NoLSA^{M}-GFP and

fusions were coexpressed with mRFP-Fib. In contrast to N55-GFP, N55NoLSA^M-GFP fusion did not localize to nucleoli or to discrete mRFP-Fib-labeled speckles, presumably the Cajal bodies (Fig. 3B, middle row), and N55NoLSB^M-GFP was partially excluded from the nucleolus (Fig. 3B, bottom row). Both fusions showed similar ratios of nucleolar to nuclear fluorescence (0.63 and 0.72) to N26-GFP and N123-GFP, but they differed significantly from N55-GFP and N84-GFP (Fig. 3C). Thus, TGB1 residues 11 to 16 and 37 to 52 act as functional NoLS.

Ala Substitution of Positively Charged Amino Acids in NoLSA and NoLSB Affects Virus Long-Distance Movement

To investigate whether mutations affecting NoLSA and NoLSB perturb virus infection, the same mutations were introduced into the full-length clone of PMTV RNA-TGB. Following inoculation with infectious transcripts of PMTV RNA-Rep, RNA-CP, and each of the mutants (collectively referred to as PMTV-NoLSA^M, PMTV-NoLSB^M, and PMTV-NoLSAB^M), RT-PCR and ELISA at 14 dpi revealed that, whereas PMTV-NoLSA^M accumulated in upper noninoculated leaves in amounts similar to the wild-type virus (Fig. 4A), the accumulation of PMTV-NoLSB^M was slightly reduced. However, in infections established with PMTV-NoLSAB^M, while RNA-TGB.NoLSAB^M moved systemically, RNA-CP failed to accumulate in the upper leaves (Fig. 4, A and B), indicating that the integrity of both NoLS motifs is needed for the long-distance movement of RNA-CP. This is consistent with the stronger effect that the 84-amino acid TGB1 N-terminal truncation had on RNA-CP systemic movement compared with RNA-TGB.Δ84 (Supplemental Fig. S1C).

To investigate whether TGB1 with altered NoLS motifs associates with the nucleolus in the course of infection, the TGB1 protein with NoLSA^M and NoLSB^M was expressed as a YFP fusion from the PMTV genome (PMTV.YFP-TGB1NoLSAB^M construct). PMTV.YFP-TGB1NoLSAB^M transcripts were coinoculated onto *N. benthamiana* leaves along with transcripts of RNA-Rep and RNA-CP. Examination of fluorescent infection sites on inoculated leaves at 14 dpi showed that the virus moved cell to cell (Fig. 4C). The YFP-TGB1NoLSAB^M fusion retained strong fluorescence in punctate structures at the cell periphery (Fig. 4E), presumably plasmodesmata (Wright at al., 2010), but was excluded from nucleoli (Fig. 4D), consistent with a dependence of nucleolar targeting on NoLSA and NoLSB.

TGB1 Associates with Importin-α in *N. benthamiana* Epidermal Cells

The ability of proteins to enter the nucleus and, in turn, the nucleolus is importin-α dependent, as importin-α shuttles between the cytoplasm and the nucleus and binds to the nuclear localization signal (NLS) of the proteins in the cytoplasm. We next determined whether full-length TGB1, truncated TGB1 variants, and N-terminal TGB1 fragments interact with *N. benthamiana* importin-α1 (IMP) by BiFC (Table III). Cells coexpressing either IMP-FP and Y-TGB1 or TGB1-FP and Y-IMP showed YFP fluorescence, which was localized to the nucleus and strongly enriched in the nucleolus, but did not label microtubules (Fig. 5A; Table III). Because no differences were observed between the reciprocal complementation pairs, N-terminal fragments of TGB1 were subsequently tested for IMP interaction in only one orientation. N26-FP, N55-FP, N84-FP, and N123-FP all showed similar nuclear fluorescence with nucleolar enrichment when coexpressed with Y-IMP (Fig. 5A; Table III). For N84, the reciprocal combination Y-N84 + IMP-FP was also tested and confirmed the localization pattern (Fig. 5A). Nucleolar enrichment was weaker for N26-GFP or N123-GFP (Fig. 3A), but in BiFC tests, the interaction with importin-α may have recruited these TGB1 fragments to the nucleolus. Additionally, we tested interactions of the truncated variants Δ84 and Δ149 (both orientations; Table III) with IMP. Neither of these combinations produced YFP fluorescence, indicating that the NTD of TGB1 is sufficient to interact with importin-α as it contains NoLSA and NoLSB (Table III). As negative controls, each of the fusion proteins was expressed on its own (alone) or in pairwise combination with Y-GST (Table III). Cells coexpressing Δ84-FP and IMP-Y, or Δ149-FP and IMP-Y, or IMP-FP and Y-Δ149 yielded no YFP fluorescent signal in the nucleoli (Table III). We concluded that the NTD of TGB1 is sufficient to interact with importin-α as it contains NoLSA and NoLSB. To further test the hypothesis that TGB1 nuclear translocation is governed by importin-α, coimmunoprecipitation (co-IP) assays were performed. *N. benthamiana* leaves were coinfiltrated with *Agrobacterium tumefaciens* strains carrying plasmids to encode TGB1-GFP and myc-tagged NbIMPα1 (myc-IMPα1) or nonfused TGB1 (TGB1) and myc-IMPα1. The protein extracts were subjected to immunoprecipitation with anti-GFP microbeads. Our results showed that myc-IMPα1 could be coimmunoprecipitated by anti-GFP antibody in the presence of TGB1-GFP and could not be coimmunoprecipitated in the presence of nonfused TGB1 (Fig. 5B). These results confirmed that TGB1 associates with importin-α in planta.

Figure 3. (*Continued.*)
N55NoLSB^M-GFP, respectively). GFP is shown in green, and the nucleolar marker, mRFP-Fib, is shown in magenta. Bars = 5 μm. C, Quantification of the nucleolar-nuclear fluorescence ratio for the four N-terminal fragments as well as N55NoLSA^M and N55NoLSB^M. Error bars represent SD ($n = 10$), and letters indicate groups of constructs that differ significantly from each other (one way-ANOVA and Dunnett's T3 test; $P < 0.001$). The table at right shows mean, SD, and range of fluorescence ratios.

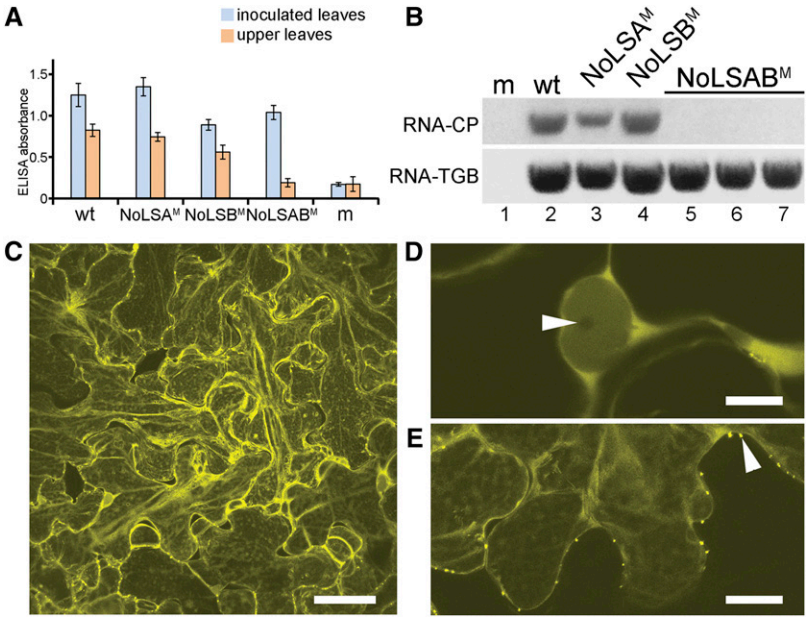

Figure 4. Effects of the Ala substitutions of the Arg and Lys residues in NoLSA, NoLSB, and both NoLS motifs on TGB1 localization and virus accumulation in inoculated and upper leaves. A, Accumulation of PMTV measured by ELISA as indicated by absorbance values at 405 nm. Plant extracts were prepared from inoculated and upper leaves 14 dpi. The average absorbance of a healthy plant extract (m, mock) was equal to 0.17. ELISA experiments were conducted twice (n = 6). Error bars denote SD. wt, Wild type. B, RT-PCR on RNA of *N. benthamiana* upper leaves to detect the accumulation of viral RNA-CP and RNA-TGB. The identity of each virus inoculum is indicated above the gels (lanes 5–7 are different plants inoculated with PMTV-NoLSAB^M). Thirty cycles were used for amplification. The experiment was repeated twice with similar results. C, Multicellular lesion of PMTV.YFP-TGB1NoLSAB^M 14 dpi showing cell-to-cell movement of the mutant virus. Bar = 40 μm. D, Localization of YFP-TGB1NoLSAB^M to the nucleolus upon expression from the viral genome. Bar = 5 μm. E, Single confocal section illustrating YFP-TGB1NoLSAB^M located in punctate structures (arrowhead) in the cell wall, presumably plasmodesmata. Bar = 5 μm.

We then tested whether full-length TGB1 with the NoLSA^M, NoLSB^M, or NoLSAB^M amino acid substitution in NoLSs (Fig. 1) interacts with importin-α. In the BiFC system, reconstituted YFP fluorescence was detected in the nuclei but not in the nucleoli (Table III; Fig. 5A). Coexpression of NoLSA^M-FP and IMP-Y revealed very weak yellow fluorescence in only 14 cells out of 78 examined (18% of the cells; Table III), indicating that the NoLSA^M protein was mostly excluded from the nucleolus. Nucleolar localization of GFP-fused importin-α was verified by coexpression with mRFP-Fib (Fig. 5C). These data indicate that the TGB1 N terminus mediates the interaction of TGB1 with importin-α and that the NoLSA and NoLSB motifs play a role in nucleolar targeting of the TGB1-importin-α complex.

Knockdown of the Expression of Two Importin-α Homologs, *NbImp-α1* and *NbImp-α2*, Results in Partial Suppression of Systemic PMTV Infection

To further confirm the role of importin-α in the nucleolar localization of TGB1, which, in turn, is necessary for efficient PMTV systemic infection, we carried out virus-induced gene silencing (VIGS) of *NbImp-α1* and *NbImp-α2* genes and engineered a novel reporter clone of PMTV. The previously reported modified viruses, PMTV.GFP-TGB1 and PMTV.YFP-TGB1, can efficiently move cell to cell but are unable to move systemically and, therefore, are not suitable to study the virus systemic infection (Zamyatnin et al., 2004; Wright et al., 2010). To overcome this limitation, the GFP sequence in PMTV.GFP-TGB1 was replaced with a shorter sequence for the myc tag. The myc-tagged virus, PMTV.myc-TGB1, was inoculated on *N. benthamiana* and compared with the wild-type virus. The inoculated plants developed symptoms typical of PMTV infection 14 dpi, and the timing of the symptoms and their appearance were similar to those of the wild-type virus (Supplemental Fig. S2A). Moreover, the rates of PMTV systemic movement and virus accumulation in upper leaves were similar to those of the wild type (Supplemental Fig. S2B), and myc-tagged TGB1 could be readily detected in upper leaves by immunoblot analysis (Fig. 6A). From these results, we concluded that PMTV.myc-TGB1 is suitable for studies of virus infection in the whole plant.

The two importin-α paralogs in *N. benthamiana* were silenced with the Tobacco rattle virus (TRV)-based VIGS system. Two 0.3-kb fragments of *NbImp-α1* and *NbImp-α2* complementary DNAs (cDNAs) were amplified and cloned into the TRV:00 vector in an antisense orientation. *N. benthamiana* seedlings (at the four-leaf stage) were infiltrated with *A. tumefaciens* strains carrying TRV constructs. An empty TRV vector (TRV:00) was used as

Table III. *Interactions assayed by BiFC*

Construct Pairs Tested	Microtubules	Nucleus	Nucleolus
TGB1-FP + Y-IMP	−	+	+
IMP-FP + Y-TGB1	−	+	+
N26-FP + Y-IMP	−	+	+
N55-FP + Y-IMP	−	+	+
N84-FP + Y-IMP	−	+	+
IMP-FP + Y-N84	−	+	+
N123-FP + Y-IMP	−	+	+
N26-FP + Y-GST	−	−	−
N55-FP + Y-GST	−	−	−
N84-FP + Y-GST	−	−	−
N123-FP + Y-GST	−	−	−
IMP-FP + Y-GST	−	−	−
GST-FP + Y-GST	−	−	−
Δ84-FP + IMP-Y	−	−	−
Δ84-FP + Y-TGB1	+	+	+
IMP-FP + Y-Δ149	−	−	−
Δ149-FP + Y-IMP	−	−	−
NoLSA^{M}-FP + Y-IMP	−	+	+[a]
NoLSB^{M}-FP + Y-IMP	−	+	−
NoLSAB^{M}-FP + Y-IMP	−	+	−

[a]Weak interaction detected in 14 cells out of 78.

a control. At 14 d after infiltration, leaf samples were collected, total RNA was extracted, and silencing of the *NbImp-α* genes was verified by RT-PCR (Fig. 6B). Ten plants for each construct were assayed in two independent experiments. The RT-PCR results showed significantly lower levels of amplification for *NbImp-α* transcripts in the TRV:*Imp-α1*- and TRV:*Imp-α2*-treated plants compared with the control samples, whereas the amplification levels of the *N. benthamiana* translation elongation factor1α transcripts were similar in all samples analyzed (Fig. 6B). Therefore, the results suggested that the *NbImp-α* genes were silenced in *N. benthamiana* leaves. Interestingly, infections with TRV:*Imp-α1* did not result in silencing of the second gene (*NbImp-α2*) and vice versa (Fig. 6B), presumably indicative of the high specificity of the silencing constructs.

At this time point, the *N. benthamiana* plants agroinfiltrated with empty TRV:00 vector and the plants silenced for the *NbImp-α* genes were inoculated with PMTV.myc-TGB1. Quantitative analysis of PMTV accumulation 14 dpi revealed that the ELISA absorbance values of PMTV progeny were approximately 20% lower in upper leaves of plants silenced for the *NbImp-α* genes (either *Imp-α1* or *Imp-α2*) as compared with those of plants challenged with empty VIGS vector (Fig. 6C). Interestingly, some plants were found to be negative for the presence of PMTV CP antigen according to ELISA. Total RNA was extracted from upper leaves of these plants and analyzed by RT-PCR for the presence of RNA-TGB and RNA-CP. The RT-PCR results showed a lack of amplification for RNA-CP in these plants, while the high amplification levels of RNA-TGB were obtained in all samples analyzed (Fig. 6D). Therefore, the results suggest the selective loss of RNA-CP movement in *N. benthamiana* plants silenced for the importin-α genes, a phenomenon similar to previous reports for RNA-CP mutants, which express C terminally truncated CP-RT protein unable to interact with TGB1 (Torrance et al., 2009).

To determine the effect of the *NbImp-α* gene silencing on myc-TGB1 accumulation in the nucleus, we performed subcellular fractionation and anti-myc immunoblotting (Fig. 6E). Whereas the myc-TGB1 protein was detected in the nuclear P10 fraction in both silenced and nonsilenced plants (Fig. 6E; Supplemental Fig. S2C), significantly less ($P < 0.01$; Student's t test) myc-TGB1 protein was detected in the nuclei of the plants silenced for the *NbImp-α* genes (on average, $n = 5$; 26% and 16.5% of the total myc-TGB1 protein in the S30 and P10 fractions combined for *Imp-α1*- and *Imp-α2*-silenced plants, respectively) as compared with the control nonsilenced plants (on average, 44%; $n = 5$) agroinfiltrated with empty TRV:00 vector (Fig. 6F; Supplemental Fig. S2C). From these results, it was apparent that the interaction of TGB1 with nuclear transport receptors of the importin-α family is needed for targeting to the nucleolus and, ultimately, for efficient systemic infection/movement of PMTV.

DISCUSSION

Positive-strand RNA viruses replicate in the cytoplasm in large intracellular membrane-associated complexes (Nagy and Pogany, 2011). However, some viruses encode proteins that target the nucleus, a feature common to an increasing number of plant positive-strand RNA viruses (Solovyev and Savenkov, 2014). These proteins contain NLS motifs and protein-protein and protein-nucleic acid (RNA and/or DNA) interaction domains that allow them to bind to host promoters (Lukhovitskaya et al., 2013a) or to recruit the viral RNA, other viral proteins, and/or host factors to facilitate viral cell-to-cell and/or systemic movement through the phloem (see references below). Well-characterized plant virus proteins of this category include the ORF3 protein of *Groundnut rosette virus* (GRV; unassigned family, genus *Umbravirus*), the CP of *Potato leaf roll virus* (family Luteoviridae), the genome-linked viral protein of *Potato virus A* (family Potyviridae), the 2b suppressor of RNA silencing of *Cucumber mosaic virus* (family Bromoviridae), the P7a movement protein of *Beet black scorch virus* (family Tombusviridae), the CP of *Alfalfa mosaic virus* (family Bromoviridae), the P30 movement protein encoded by *Turnip vein clearing virus* (family Virgaviridae), and the P14 suppressor of RNA silencing and P25 of *Beet necrotic yellow vein virus* (family Virgaviridae; Haupt et al., 2005b; Kim et al., 2007; Rajamäki and Valkonen, 2009; González et al., 2010; Herranz et al., 2012; Wang et al., 2012; Chiba et al., 2013; Levy et al., 2013). Other viral proteins found in the nucleolus include the P3 protein of *Tobacco etch virus* (family Potyviridae) and the CP of *Ourmia melon virus* (unassigned family, genus *Ourmiavirus*), but the function of these nucleolar localizations is unknown (Taliansky et al., 2010; Crivelli et al., 2011; Rossi et al., 2014). Another nucleolus-localized

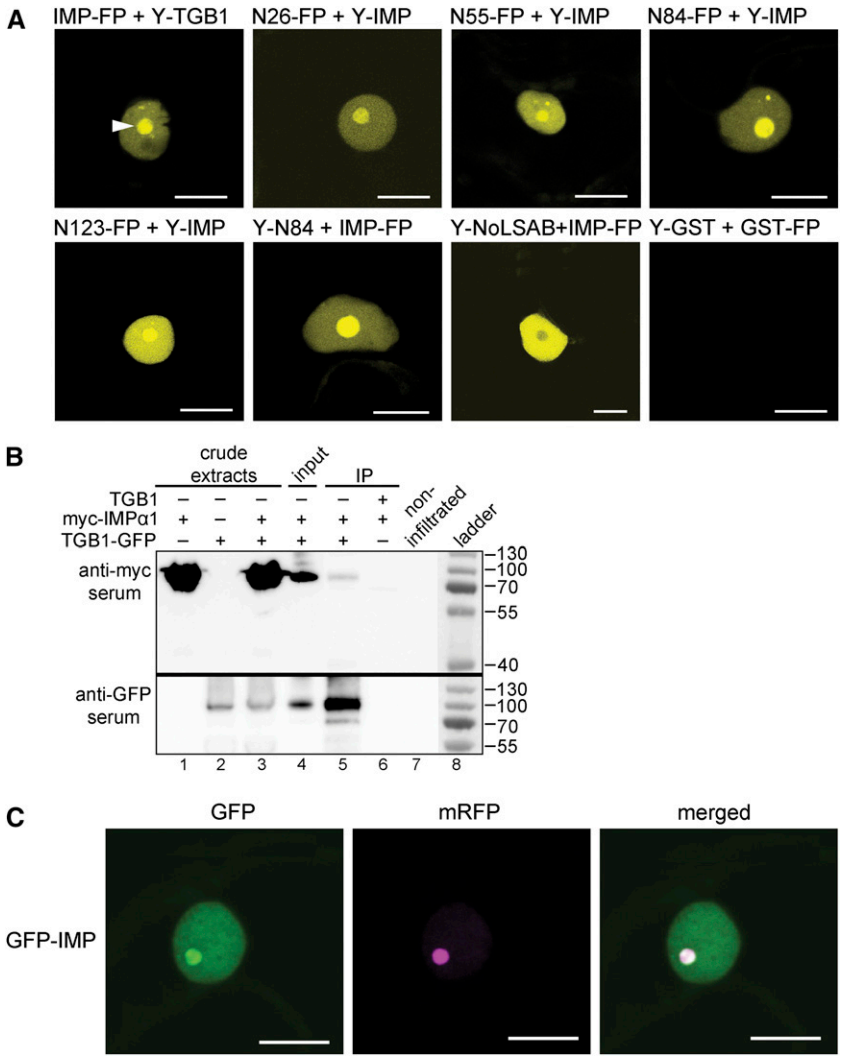

Figure 5. Importin-α interacts with the PMTV TGB1 protein. Interactions were assayed by BiFC and co-IP. A, TGB1 fused to the N-terminal half of YFP and NbImp-α1 fused to the C-terminal half of YFP transiently coexpressed in epidermal cells of *N. benthamiana* show reconstituted fluorescence of YFP in the nucleoplasm and accumulation of fluorescence at the nucleolus. TGB1 N-terminal fragments (26, 55, 84, and 123 residues) fused to the C-terminal half of YFP and NbImp-α1 fused to the N-terminal half of YFP (Y-IMP) show reconstituted YFP fluorescence in the nucleoplasm and accumulation at the nucleolus. Cells coexpressing TGB1 altered in both NoLSs (NoLSAB^{M}) fused to the N-terminal half of YFP and NbImp-α1 fused to the C-terminal half of YFP show reconstituted YFP fluorescence in the nucleoplasm and partial exclusion from the nucleolus. The BiFC control with GST fused to the N-terminal and C-terminal halves of YFP shows no reconstituted fluorescence. For all tested BiFC combinations, see Table III. B, Co-IP of extracts from *N. benthamiana* leaves coinfiltrated with TGB1-GFP and myc-IMPα1, or TGB1 and myc-IMPα1, using anti-GFP microbeads, followed by immunoblot analysis with anti-myc and anti-GFP antibodies (lanes 4–6). The coexpression of nonfused TGB1 and myc-IMPα1 was used as a control in the co-IP experiment (expression controls for the proteins; lanes 1–3). The experiments were conducted twice. C, GFP-IMPα1 (green) coexpression with mRFP-Fib (magenta). Bars = 5 μm.

movement protein, the TGB1 protein of PMTV, is the subject of this study. Although much progress has been made in characterizing the nucleolus-localized proteins and the general nucleolar entry strategies of different viruses, many of the molecular details remain obscure.

PMTV TGB1 is required for cell-to-cell and systemic movement and appears to be an essential component of long-distance movement-competent virions (Zamyatnin et al., 2004; Torrance et al., 2009). The loss of TGB1 interaction with the CP-RT protein (another nonstructural component of virions) through C-terminal truncations of CP-RT results in inefficient systemic movement of the virus and a lack of RNA-CP movement to the upper leaves (Torrance et al., 2009; Wright et al., 2010). Moreover, the deficiency of the Δ84 mutant in long-distance movement correlates with the inability of the altered TGB1, which lacks 84 amino acids from the N terminus, to enter the nucleolus (Wright et al., 2010). Previously, we hypothesized that this 84-amino acid fragment might contain a NoLS (Wright et al., 2010). The study reported here investigates the function of the two domains, NTD and the internal domain, of PMTV TGB1 (Table I), in the processes of nucleolar localization and virus cell-to-cell and long-distance movement. We showed that two amino acid stretches, namely 11-HRVKKD-16 and 37-FRTNNNKKTQNWKPRS-52, contain motifs required for nucleolar interaction with importin-α and efficient long-distance movement.

Localization of PMTV TGB1 in the nucleolus was reported previously using translational GFP and YFP fusions of TGB1 and confocal laser scanning microscopy (Wright et al., 2010). Here, we mapped two regions involved in targeting PMTV TGB1 to the nucleolus. We demonstrated that the Arg residue at position 12 and two Lys residues at positions 14 and 15 within the 11-H**R**V**KK**D-16 sequence and two Arg residues and three Lys residues within the 37-F**R**TNNN**KK**TQNW**K**P**R**S-52 sequence are sufficient and critical for nucleolar targeting and, thus, were defined and annotated as NoLSA and NoLSB, respectively. Experiments using infectious clones of the virus and single and double mutants for NoLS demonstrated that, whereas single mutants were able to

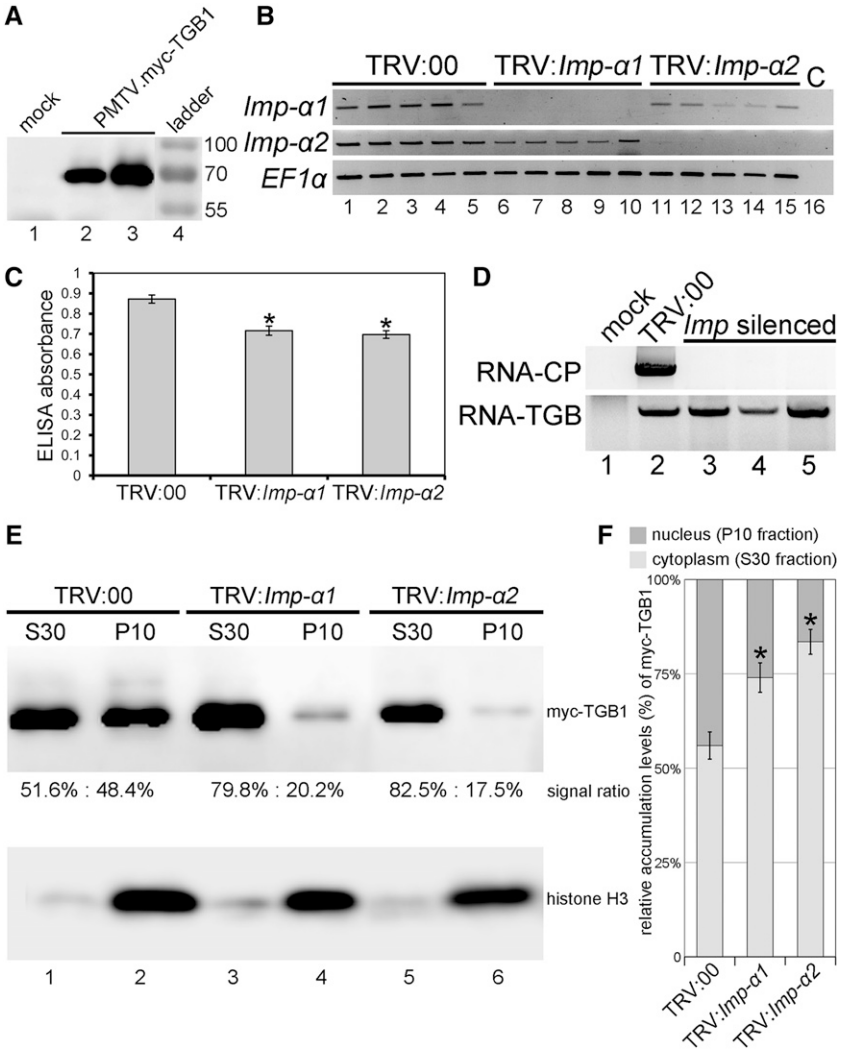

Figure 6. Effects of the knockdown of the expression of two importin-α homologs on PMTV accumulation in upper noninoculated leaves. A, Immunoblot analysis of c-myc epitope-tagged TGB1 expressed from the virus. At 14 dpi, samples from upper noninoculated leaves were analyzed by immunoblot using anti-myc antibody. Positions of protein standards (in kD) are marked at right. B, RT-PCR of RNA from 4-week-old *N. benthamiana* plants inoculated with TRV:*Imp-α1* or TRV:*Imp-α2* silencing constructs or with an empty VIGS vector (TRV:00). Primers detect *Importin-α1*, *Importin-α2*, or *EF-1α* transcripts. Each lane corresponds to a different plant. C, Levels of PMTV accumulation detected by ELISA as indicated by absorbance values at 405 nm. Plant extracts were prepared from upper leaves 14 dpi. The average absorbance of a healthy plant extract was equal to 0.14. Asterisks indicate that the absorbance values were significantly different ($P < 0.05$; Student's *t* test) from those of nonsilenced control plants (TRV:00). Experiments were conducted twice ($n = 10$). D, RT-PCR analysis of RNA from *Importin-α1*-silenced plants (lanes 3 and 4) and *Importin-α2*-silenced plants (lane 5), which were completely negative for the presence of PMTV CP antigen in ELISA, using primers to detect PMTV RNA-CP or PMTV RNA-TGB. RNA samples from the upper leaves of a mock-inoculated plant or from the upper leaves of a plant inoculated with empty VIGS vector (TRV:00) served as controls. E, Presence of c-myc-tagged TGB1 in the nuclear P10 and cytoplasmic S30 fractions. The fractions were analyzed by immunoblotting using antisera to the c-myc-tag (top) and to histone H3 as a nuclear marker (bottom). The relative extent of myc-TGB1 signal in the nuclear and cytoplasmic fractions is shown below the top gel. F, Relative myc-TGB1 accumulation levels were measured on immunoblots in two independent experiments ($n = 5$). Additional images used for quantification are shown in Supplemental Figure S2C. Asterisks indicate statistically significant differences compared with the control group, TRV:00 ($P < 0.01$; Student's *t* test).

move systemically similar to the wild type, PMTV RNA-CP failed to move to the upper leaves in the double mutant, implying that two other viral RNAs, RNA-Rep and RNA-TGB.NoLSAB, moved systemically as a vRNP and that the integrity of both NoLS motifs is required for efficient long-distance transport of RNA-CP. Consistent with these observations, altered TGB1 protein (which lacks both NoLSs) expressed as a translational fusion with YFP from the infectious virus clone did not enter the nucleolus.

Two general mechanisms have been described for nuclear import: passive diffusion and facilitated translocation. Whether passive diffusion contributes to the nucleolar entry of the proteins is not known, whereas facilitated nuclear as well as nucleolar import requires the presence of either NLS or NoLS. The nuclear and nucleolar import of NoLS-bearing proteins is mediated by a heterodimer nuclear-cytoplasmic-shuttling receptor consisting of importin-α and importin-β. These data suggest that the accumulation of TGB1 in the nucleus and its targeting to the nucleolus might be mediated by an importin-dependent mechanism. This hypothesis is in agreement with the observations that (1) depletion of importin-α though VIGS resulted in reduced TGB1 accumulation in the nucleus and (2) six point mutations resulting in three amino acid substitutions in TGB1 NoLSA could change the nucleolar transport requirements of TGB1, as this altered protein still had intact NoLSB. Partial, but not complete, depletion of TGB1 in the nucleolus and, as the result of that, partial suppression of PMTV infection in upper leaves by knockdown of two importin-α homologs, *NbImp-α1* and *NbImp-α2*, suggest that other α-importins might work redundantly with importin-α1 and importin-α2 in TGB1 translocation to the nucleus and nucleolus. High levels of redundancy in the nuclear import of viral proteins were shown for many other viruses, such as for the nucleoprotein of influenza virus A (O'Neill et al., 1995; Melen et al., 2003; König et al., 2010). Nucleoprotein binds to a number of human importin-α proteins (O'Neill et al., 1995; Melen et al., 2003). Additionally, a genome-wide RNA interference screen identified transportin3 as a host factor required for influenza virus A replication in human cells (König et al., 2010), suggesting that, besides the classical importin-α/importin-β pathway, other nuclear import pathways may be involved. Similarly, our results suggest that highly redundant proteins of the importin family might be involved in the nucleolar transport of PMTV TGB1, as knockdown of either importin-α1 or importin-α2 did not entirely abolish TGB1 accumulation in the nucleus. This could also explain why importin-α silencing resulted in only a small reduction in PMTV systemic movement. Indeed, whereas the Arabidopsis genome contains nine genes that encode importin-α, our mining of the Sol Genomics Network database retrieved 14 importin-α-like proteins of *N. benthamiana*. A phylogenetic analysis of these importin-α-related proteins revealed that they formed three distinct clades (I–III) in the phylodendrogram with a high statistical probability (bootstrap values $> 70\%$; Supplemental Fig. S3; Supplemental Data Set S1). Notably, each of the NbImp-α1 and NbImp-α2 subclades contain three close homologs (Supplemental Fig. S3). Overall, this analysis suggests a high level of redundancy among importin-α isoforms in *N. benthamiana*. Since importin-α is encoded by a multigene family in *N. benthamiana*, this might explain why silencing of *NbImp-α1* and *NbImp-α2* decreased but did not entirely abolish TGB1 accumulation in the nucleus.

Moreover, using co-IP, BiFC, and live cell imaging, we determined that PMTV TGB1 associates with nuclear-cytoplasmic receptor importin-α in vivo. Of the viruses that express movement proteins localized to the nucleolus, the nucleolar import of GRV is probably the best studied. The GRV genome does not encode a coat protein. While most plant RNA viruses move long distance through phloem as virus particles, GRV moves as a vRNP. In this complex, ORF3 cooperatively binds viral RNA to enable vRNP long-distance movement (Kim et al., 2007).

Experiments using several PMTV RNA-TGB mutants, which express N terminally truncated TGB1, demonstrated that amino acid residues 1 to 149 of the NTD are dispensable for virus cell-to-cell movement but required for efficient systemic movement. Strikingly, cell-to-cell movement of the PMTV mutants positively correlated with the ability of the truncated TGB1 variants to self-interact, suggesting that TGB1 protein-protein interactions might be needed for the formation of cell-to-cell movement-competent vRNPs assembled from viral RNA and TGB1 through cooperative binding. As cooperative binding of proteins to nucleic acids involves two types of interactions, namely, nucleic acid-protein and protein-protein interactions, these results are consistent with previously reported roles of the internal domain of BSMV TGB1 in binding ssRNA in a cooperative manner (Makarov et al., 2009). Indeed, all three truncated TGB1 variants capable of self-interaction had the internal domain preserved. Two other PMTV RNA-TGB mutants, which express truncated TGB, partially (Δ169) or entirely (Δ249) lacking the internal domain, were unable to move cell to cell. In support of this finding, the TGB1 internal domain was predicted by PSS Finder and by Phyre 2 (Kelley and Sternberg, 2009) to form a long α-helix, which spans the region amino acids 161 to 180 (Table I). Interestingly, the Δ169 mutant expresses TGB1 protein with most of this α-helix deleted, suggesting that the α-helix might mediate TGB1 oligomerization (dimerization). Collectively, these data further support the idea (Makarov et al., 2009) of a three-domain organization (NTD, internal domain, and helicase domain) of hordeivirus-like TGB1 proteins and that interaction between these domains and viral RNA or virions can provide a basis for remodeling of the viral transport forms for cell-to-cell and long-distance movement. The data also emphasize the centrality and regulatory role of TGB1 in facilitating virus movement.

Taken together, these results have resolved new aspects in the functioning of the structural domains of TGB1 and their involvement in the mediation of TGB1 self-interactions and the facilitation of TGB1's association with a host receptor, importin-α. These results also showed that interactions of TGB1 with importin-α are significant to PMTV infection, as the loss of interaction often resulted in the loss of RNA-CP systemic movement and, therefore, might threaten the integrity/stability of the tripartite PMTV genome. Therefore, TGB1 seems to act in trans on RNA-CP survival/maintenance during phloem transport. Thus, nucleolar passage of TGB1 is essential for the survival of tripartite PMTV, ensuring that PMTV RNA-CP is not lost by chance or eroded from the virus genome by mutations either in the RT

region of CP-RT (Torrance et al., 2009) or in trans-acting TGB1 (Wright et al., 2010; this study).

MATERIALS AND METHODS

Plant Material, Growth Conditions, and Inoculations

Nicotiana benthamiana plants were grown with a daylength of 16.5 h, minimum daytime temperature of 20°C, and minimum nighttime temperature of 18°C. Plants were used for VIGS experiments when they were 10 to 14 d old and for protein localization studies when they were 30 to 35 d old. Infectious PMTV RNA in vitro transcripts were generated from *Mlu*I-linearized pPMTV1 (RNA-Rep), *Mlu*I-linearized pPMTV2 (RNA-CP), and *Spe*I-linearized pPMTV3 (RNA-TGB; Savenkov et al., 2003) or pPMTV3 derivatives (all *Spe*I linearized) using the RiboMAX Large Scale RNA Production System T7 kit (Promega), following the manufacturer's protocol for the synthesis of capped RNA transcripts. Transcripts were mixed with GKP buffer (50 mM Gly, 30 mM K_2HPO_4 [pH 9.4], 1% [w/v] bentonite, and 1% [w/v] celite) in a 1:1:1:1 ratio and rub inoculated onto *N. benthamiana* leaves.

Construction of Plasmids

Standard recombinant DNA procedures were carried out using a combination of PCR, site-directed mutagenesis, swapping of restriction fragments, and Gateway cloning (Invitrogen). The sequences of the primers used in this study will be provided upon request. The plasmid pPMTV-3 (full-length infectious clone of RNA-TGB; Savenkov et al., 2003) was used to generate the mutants and constructs described in this study.

The pRNA-TGB.Δ84 mutant was described previously (Wright et al., 2010). Additional deletion mutants (Δ44, Δ149, Δ169, and Δ249) were obtained in a similar manner by replacing the Δ84 sequence in the pRNA-TGB.Δ84 plasmid with the respective portions of the *TGB1* ORF digested with *Nco*I/*Kpn*I.

Yeast (*Saccharomyces cerevisiae*) expression constructs were generated using the pLex-Na and pVP16+ vectors (Hollenberg et al., 1995). The appropriate portions of the TGB1 ORF were amplified with primers introducing *Eco*RI/*Pst*I or *Apa*I/*Eco*RI restriction sites using pPMTV3 as a template. The PCR products were digested with *Eco*RI/*Pst*I or *Apa*I/*Eco*RI and cloned into the same sites of pLex-Na or pVP16+.

The constructs for the expression of GFP fusions with the N-terminal amino acid residues 26, 55, 84, and 123 of TGB1 or with the N terminally truncated 44, 84, 149, 169, and 249 amino acids were first engineered by amplifying the respective portion of the TGB1 ORF using pPMTV3 as a template in the PCR with primers attB-TGB1Nfor and attB-p1-25rev (1–26), attB-TGB1NFor and attB-p1-50rev (1–50), attB-TGB1NFor and attB-p1-84rev (1–84), or attB-TGB1NFor and attB-p1-123rev (1–123). The amplified products were recombined into pDONR207 using Gateway BP Clonase II (Invitrogen) before recombination into pGWB405 (Nakagawa et al., 2007).

pDONR207 constructs containing the sequences coding for the N-terminal 26, 55, 84, and 123 amino acid residues were recombined into pSITE-cEYFP-N1 (Martin et al., 2009) using Gateway LR Clonase II (Invitrogen).

Site-directed mutagenesis and overlap PCR were used to create the $NoLSA^M$ and $NoLSB^M$ mutations in the N55-GFP (pGWB405) construct. For $NoLSA^M$, primer pairs 35SMfeI/NoLSAR and NoLSAF/GFPSacI were used for amplification with the N55-GFP construct as a template. These products were combined in an overlap PCR using primers 35SMfeI and GFPSacI and cloned into *Mfe*I- and *Sac*I-digested N55-GFP. Site-directed mutagenesis and overlap PCR were used to create $NoLSA^M$, $NoLSB^M$, and $NoLSAB^M$ mutations in the construct pDONR207-TGB1. These mutated entry clones were recombined into pSITE-nEYFP-C1 or pSITE-cEYFP-N1 using Gateway LR Clonase II.

For co-IP analysis, full-length ORFs of *NbImp-α1* and PMTV TGB1 were subcloned into pDONR201 and then recombined into pGWB18 for *Imp-α1* and pGWB606 for *TGB1* to produce 35S promoter-driven N-terminal translational fusions with myc epitope and GFP, respectively.

To obtain TRV:*Imp-α1* and TRV:*Imp-α2* silencing constructs, *Xho*I/*Eco*RI-digested PCR products generated with Imp-α1-XhoI-FW and Imp-α1-EcoRI-R primers, or Imp-α2-XhoI-FW and Imp-α2-EcoRI-R primers, respectively, were ligated into TRV:00 digested with *Xho*I/*Eco*RI.

Yeast Two-Hybrid System

The interaction between VP16 and LexA protein fusions was examined in the yeast L40 strain [MATa his3Δ200 trp1-901 leu 2-3,112 ade2 lys2-801am URA3::$(lexAop)_8$-*lacZ*, LYS2::$(lexAop)_4$-HIS3]. Yeast cells were cotransformed by the small-scale lithium acetate yeast transformation method as described in Clontech's Yeast Protocols Handbook. Transformants were selected on synthetic dropout minimal medium base containing 2% (w/v) Glc and dropout supplements lacking Leu and Trp or –UHLW. For the agarose overlay plate assay, transformed yeast colonies growing on –UHLW medium were entirely immersed in chloroform for 5 min. The chloroform was then decanted, and the plate was allowed to dry for another 5 min. The plate was then overlaid with 1% (w/v) low-melting-point agarose supplemented with 1 mg mL^{-1} 5-bromo-4-chloro-3-indolyl-β-D-galactopyranoside in Z buffer (60 mM Na_2HPO_4•$7H_2O$, 40 mM NaH_2PO_4•H_2O, 10 mM KCl, and 1 mM $MgSO_4$•$7H_2O$, pH 7) and incubated at 28°C for 2 and 16 h before taking the photographs.

Imaging of Fluorescent Proteins

All imaging was conducted using a Leica TCS-SP2 AOBS device (Leica Microsystems). Unless stated otherwise, images were obtained using a Leica HCX APO ×63/0.9W water-dipping lens and whole lesions using an HCX PL Fluotar ×1.6/0.05 lens. GFP and YFP were imaged sequentially: For GFP, excitation was at 488 nm, and emission was at 490 to 510 nm; and for YFP, excitation was at 514 nm, and emission was at 535 to 545 nm. GFP and mRFP were imaged sequentially: For GFP, excitation was at 488 nm, and emission was at 500 to 530 nm; and for mRFP, excitation was at 561 nm, and emission was at 590 to 630 nm. Images were prepared using Adobe Photoshop CS5. For quantification of nuclear and nucleolar GFP fluorescence, mean intensity values were measured on a single confocal section for each that clearly showed the nucleolus in hand-selected regions of interest using ImageJ software. Nucleolar-nuclear fluorescence ratios were then calculated for each cell, and the different constructs were compared by one-way ANOVA followed by Dunnett's T3 test (not assuming homogeneity of variances). Statistical analysis was done using SPSS software (IBM).

Virus Detection Kit and Antibodies

The following commercial antibodies were used: anti-myc (Roche), anti-GFP (monoclonal antibody JL-8; Clontech), and anti-acetyl-histone H3 IgG (Upstate). The potato mop-top virus DAS-ELISA kit (BIOREBA) was used for the virus detection.

co-IP

Agrobacterium tumefaciens strains C58C1 (with Ti plasmid pGV3850 or pGV2260) carrying myc-IMPα1, TGB1-GFP, or hemagglutinin-tag-TGB1 was infiltrated into *N. benthamiana* leaves in the desired combinations at optical density at 600 nm = 0.5 along with an *A. tumefaciens* strain carrying potato virus A HC-Pro, a suppressor of RNA silencing, at optical density at 600 nm = 0.1 to boost the protein expression. Forty-eight hours later, leaves were ground in liquid nitrogen and total protein was extracted according to the manufacturer's recommendation (Chromtek) with lysis buffer (10 mM Tris-HCl, pH 7.5, 150 mM NaCl, 0.5 mM EDTA, 0.5% [w/v] Nonidet P-40, EDTA-free protease inhibitor mixture [Roche], and 1 mM phenylmethylsulfonyl fluoride) at a fresh weight:buffer ratio of 100 mg:100 μL. Samples were incubated on ice for 30 min with extensive pipetting every 10 min. After centrifugation at 20,000*g* for 10 min at 4°C, 15 to 20 μL of anti-GFP microbeads was added to the resultant supernatant and incubated for 1 h at 4°C on a rotating wheel. Subsequent washing and elution steps were performed according to the manufacturer's recommendations (GFP-Trap_M Kit; Chromtek). Protein samples were eluted in 2× Laemmli sample buffer, boiled for 10 min, centrifuged at 17,000*g* for 10 min, and subjected to immunoblotting.

Protein Analysis, SDS-PAGE, and Immunoblotting

Equal amounts of leaf material were homogenized in protein extraction buffer (4 M urea, 100 mM dithiothreitol, and 1% [v/v] Triton X-100) and incubated on ice for 10 min. Protein samples were mixed 1:1 (v/v) with 2× Laemmli sample buffer, boiled for 10 min, and centrifuged at 13,000 rpm for 10 min. Samples were run on 12% [w/v] SDS-PAGE gels. Proteins were separated, transferred to polyvinyl difluoride membranes (Amersham Hybond-P; GE Healthcare), and blocked with 5% (w/v) nonfat milk powder in phosphate-buffered saline containing 0.05% (v/v) Tween 20. GFP-TGB1, myc-IMPα1, or myc-TGB1 was detected by the antibodies described above at final dilutions of 1:1,000. The immunoreaction was developed using the

ECL Prime kit (Amersham, GE Healthcare) and detected in a LAS-3000 Luminescent Image Analyzer (Fujifilm, Fuji Photo Film).

VIGS

Construction of the TRV:*Imp-α1* and TRV:*Imp-α2* silencing plasmids is described above. The 300-bp *Imp-α1* and *Imp-α2* fragments were cloned in an antisense orientation into the TRV:*GFP* vector by replacing the *GFP* gene. The resulting constructs, TRV:*Imp-α1* and TRV:*Imp-α2*, were transformed into *A. tumefaciens* and, in combination with TRV-RNA1, used for the induction of *NbImp-α1* and *NbImp-α2* gene silencing, respectively. Fourteen days after TRV infiltration, *N. benthamiana* leaves were challenged with PMTV.myc-TGB1. The uppermost leaves were assayed for *NbImp-α1* and *NbImp-α2* gene silencing by RT-PCR and for PMTV infection by ELISA and RT-PCR.

RT-PCR

RNA was purified from leaf pieces using the Spectrum Plant Total RNA Kit (Sigma) and On-column DNaseI Digest Set (Sigma) according to the manufacturer's instructions. Total RNA samples of 1-μg aliquots were used for cDNA synthesis with PMTV-specific primer, which anneals to the 3′ end of viral RNAs, and with the RevertAid H Minus First Strand cDNA Synthesis Kit (MBI Fermentas). The obtained cDNAs were used as templates for PCR with DreamTaq DNA Polymerase (MBI Fermentas).

Subcellular Fractionation of Plant Extracts

Subcellular fractionation of the leaf extracts was carried out as described previously (Lukhovitskaya et al., 2013a).

Data Statistical Analysis

Each experiment was performed at least in triplicate and repeated at least two times, and values are represented as means ± SD. Student's *t* test was used to determine the differences between experimental and control groups, requiring $P < 0.05$ (or $P < 0.01$) for statistical significance.

Phylogenetic and Sequence Analyses

The sequences for *N. benthamiana* importin-α proteins were retrieved from the Sol Genomics Network database (http://solgenomics.net/tools/blast/index.pl). The sequences were aligned using the ClustalW algorithm of the Megalign module of the Lasergene software package (DNASTAR), and the tree was prepared in MEGA6 (Tamura et al., 2013). Bootstrap values were calculated from 10,000 replicates of the tree. GenBank and Sol Genomics Network accession numbers are indicated on the phylodendrogram.

Algorithms Used for Bioinformatics

The following algorithms were used: Phyre 2, Protein Homology/Analogy Recognition Engine (Kelley and Sternberg, 2009), http://www.sbg.bio.ic.ac.uk/phyre2/html/page.cgi?id=index; PDISORDER, Protein Disorder Prediction, http://www.softberry.com/berry.phtml?topic=index&group=programs&subgroup=propt; IUPred, Prediction of Intrinsically Unstructured Proteins (Dosztányi et al., 2005), http://iupred.enzim.hu/; NoD, Nucleolar Localization Sequence Detector (Scott et al., 2011), http://www.compbio.dundee.ac.uk/www-nod/; and RONN to predict protein disorder (Thomson and Esnouf, 2004, Yang et al., 2005), https://app.strubi.ox.ac.uk/RONN/?p=RONN&HTTP_VARS=.

Supplemental Data

The following supplemental materials are available.

Supplemental Figure S1. Effects of the 5′ proximal deletions in the TGB1 cistron on virus accumulation in inoculated and upper leaves and on interactions of the truncated TGB1 derivatives.

Supplemental Figure S2. Characterization of the PMTV.myc-TGB1 construct.

Supplemental Figure S3. Phylodendrogram of the 14 *N. benthamiana* importin-α isoforms.

Supplemental Data Set S1. Sequences used to generate the phylodendrogram in Supplemental Figure S3.

ACKNOWLEDGMENTS

We thank Panagiotis N. Moschou (Department of Plant Biology, Swedish University of Agricultural Sciences) for technical advice concerning co-IP assays.

Received December 3, 2014; accepted January 8, 2015; published January 9, 2015.

LITERATURE CITED

Arif M, Torrance L, Reavy B (1995) Acquisition and transmission of potato mop-top furovirus by a culture of *Spongospora subterranea* f.sp *subterranea* derived from a single cystosorus. Ann Appl Biol **126:** 493–503

Barneche F, Steinmetz F, Echeverría M (2000) Fibrillarin genes encode both a conserved nucleolar protein and a novel small nucleolar RNA involved in ribosomal RNA methylation in Arabidopsis thaliana. J Biol Chem **275:** 27212–27220

Chiba S, Hleibieh K, Delbianco A, Klein E, Ratti C, Ziegler-Graff V, Bouzoubaa S, Gilmer D (2013) The benyvirus RNA silencing suppressor is essential for long-distance movement, requires both zinc-finger and NoLS basic residues but not a nucleolar localization for its silencing-suppression activity. Mol Plant Microbe Interact **26:** 168–181

Crivelli G, Ciuffo M, Genre A, Masenga V, Turina M (2011) Reverse genetic analysis of Ourmiaviruses reveals the nucleolar localization of the coat protein in Nicotiana benthamiana and unusual requirements for virion formation. J Virol **85:** 5091–5104

Dosztányi Z, Csizmok V, Tompa P, Simon I (2005) IUPred: web server for the prediction of intrinsically unstructured regions of proteins based on estimated energy content. Bioinformatics **21:** 3433–3434

González I, Martínez L, Rakitina DV, Lewsey MG, Atencio FA, Llave C, Kalinina NO, Carr JP, Palukaitis P, Canto T (2010) Cucumber mosaic virus 2b protein subcellular targets and interactions: their significance to RNA silencing suppressor activity. Mol Plant Microbe Interact **23:** 294–303

Haupt S, Cowan GH, Ziegler A, Roberts AG, Oparka KJ, Torrance L (2005a) Two plant-viral movement proteins traffic in the endocytic recycling pathway. Plant Cell **17:** 164–181

Haupt S, Stroganova T, Ryabov E, Kim SH, Fraser G, Duncan G, Mayo MA, Barker H, Taliansky M (2005b) Nucleolar localization of potato leafroll virus capsid proteins. J Gen Virol **86:** 2891–2896

Herranz MC, Pallas V, Aparicio F (2012) Multifunctional roles for the N-terminal basic motif of alfalfa mosaic virus coat protein: nucleolar/cytoplasmic shuttling, modulation of RNA-binding activity, and virion formation. Mol Plant Microbe Interact **25:** 1093–1103

Hollenberg SM, Sternglanz R, Cheng PF, Weintraub H (1995) Identification of a new family of tissue-specific basic helix-loop-helix proteins with a two-hybrid system. Mol Cell Biol **15:** 3813–3822

Jones RAC, Harrison BD (1969) The behaviour of potato mop-top virus in soil and evidence for its transmission by *Spongospora subterranea* (Wallr.) Lagerh. Ann Appl Biol **63:** 1–17

Kelley LA, Sternberg MJE (2009) Protein structure prediction on the Web: a case study using the Phyre server. Nat Protoc **4:** 363–371

Kim SH, Ryabov EV, Kalinina NO, Rakitina DV, Gillespie T, MacFarlane S, Haupt S, Brown JW, Taliansky M (2007) Cajal bodies and the nucleolus are required for a plant virus systemic infection. EMBO J **26:** 2169–2179

König R, Stertz S, Zhou Y, Inoue A, Hoffmann HH, Bhattacharyya S, Alamares JG, Tscherne DM, Ortigoza MB, Liang Y, et al (2010) Human host factors required for influenza virus replication. Nature **463:** 813–817

Levy A, Zheng JY, Lazarowitz SG (2013) The tobamovirus turnip vein clearing virus 30-kilodalton movement protein localizes to novel nuclear filaments to enhance virus infection. J Virol **87:** 6428–6440

Lukhovitskaya NI, Solovieva AD, Boddeti SK, Thaduri S, Solovyev AG, Savenkov EI (2013a) An RNA virus-encoded zinc-finger protein acts as a plant transcription factor and induces a regulator of cell size and proliferation in two tobacco species. Plant Cell **25:** 960–973

Lukhovitskaya NI, Thaduri S, Garushyants SK, Torrance L, Savenkov EI (2013b) Deciphering the mechanism of defective interfering RNA (DI RNA) biogenesis reveals that a viral protein and the DI RNA act antagonistically in virus infection. J Virol **87:** 6091–6103

Makarov VV, Rybakova EN, Efimov AV, Dobrov EN, Serebryakova MV, Solovyev AG, Yaminsky IV, Taliansky ME, Morozov SY, Kalinina NO (2009) Domain organization of the N-terminal portion of hordeivirus movement protein TGBp1. J Gen Virol **90:** 3022–3032

Martin K, Kopperud K, Chakrabarty R, Banerjee R, Brooks R, Goodin MM (2009) Transient expression in *Nicotiana benthamiana* fluorescent marker lines provides enhanced definition of protein localization, movement and interactions *in planta*. Plant J **59:** 150–162

Melen K, Fagerlund R, Franke J, Kohler M, Kinnunen L, Julkunen I (2003) Importin alpha nuclear localization signal binding sites for STAT1, STAT2, and influenza A virus nucleoprotein. J Biol Chem **278:** 28193–28200

Nagy PD, Pogany J (2011) The dependence of viral RNA replication on co-opted host factors. Nat Rev Microbiol **10:** 137–149

Nakagawa T, Suzuki T, Murata S, Nakamura S, Hino T, Maeo K, Tabata R, Kawai T, Tanaka K, Niwa Y, et al (2007) Improved Gateway binary vectors: high-performance vectors for creation of fusion constructs in transgenic analysis of plants. Biosci Biotechnol Biochem **71:** 2095–2100

O'Neill RE, Jaskunas R, Blobel G, Palese P, Moroianu J (1995) Nuclear import of influenza virus RNA can be mediated by viral nucleoprotein and transport factors required for protein import. J Biol Chem **270:** 22701–22704

Rajamäki ML, Valkonen JP (2009) Control of nuclear and nucleolar localization of nuclear inclusion protein a of picoRNA-like *Potato virus A* in *Nicotiana* species. Plant Cell **21:** 2485–2502

Reavy B, Arif M, Cowan GH, Torrance L (1998) Association of sequences in the coat protein/readthrough domain of potato mop-top virus with transmission by Spongospora subterranea. J Gen Virol **79:** 2343–2347

Rossi M, Genre A, Turina M (2014) Genetic dissection of a putative nucleolar localization signal in the coat protein of ourmia melon virus. Arch Virol **159:** 1187–1192

Sandgren M, Savenkov EI, Valkonen JPT (2001) The readthrough region of potato mop-top virus (PMTV) coat protein encoding RNA, the second largest RNA of PMTV genome, undergoes structural changes in naturally infected and experimentally inoculated plants. Arch Virol **146:** 467–477

Savenkov EI, Germundsson A, Zamyatnin AA Jr, Sandgren M, Valkonen JPT (2003) Potato mop-top virus: the coat protein-encoding RNA and the gene for cysteine-rich protein are dispensable for systemic virus movement in Nicotiana benthamiana. J Gen Virol **84:** 1001–1005

Savenkov EI, Sandgren M, Valkonen JPT (1999) Complete sequence of RNA 1 and the presence of tRNA-like structures in all RNAs of Potato mop-top virus, genus Pomovirus. J Gen Virol **80:** 2779–2784

Scott MS, Troshin PV, Barton GJ (2011) NoD: a nucleolar localization sequence detector for eukaryotic and viral proteins. BMC Bioinformatics **12:** 317–324

Solovyev AG, Savenkov EI (2014) Factors involved in the systemic transport of plant RNA viruses: the emerging role of the nucleus. J Exp Bot **65:** 1689–1697

Taliansky ME, Brown JW, Rajamäki ML, Valkonen JP, Kalinina NO (2010) Involvement of the plant nucleolus in virus and viroid infections: parallels with animal pathosystems. Adv Virus Res **77:** 119–158

Tamura K, Stecher G, Peterson D, Filipski A, Kumar S (2013) MEGA6: Molecular Evolutionary Genetics Analysis version 6.0. Mol Biol Evol **30:** 2725–2729

Thomson R, Esnouf RM (2004) Prediction of natively disordered regions in proteins using a bio-basis function neural network. Lecture Notes in Computer Science **3177:** 108–116

Torrance L, Lukhovitskaya NI, Schepetilnikov MV, Cowan GH, Ziegler A, Savenkov EI (2009) Unusual long-distance movement strategies of Potato mop-top virus RNAs in *Nicotiana benthamiana*. Mol Plant Microbe Interact **22:** 381–390

Wang X, Zhang Y, Xu J, Shi L, Fan H, Han C, Li D, Yu J (2012) The R-rich motif of Beet black scorch virus P7a movement protein is important for the nuclear localization, nucleolar targeting and viral infectivity. Virus Res **167:** 207–218

Wright KM, Cowan GH, Lukhovitskaya NI, Tilsner J, Roberts AG, Savenkov EI, Torrance L (2010) The N-terminal domain of PMTV TGB1 movement protein is required for nucleolar localization, microtubule association, and long-distance movement. Mol Plant Microbe Interact **23:** 1486–1497

Yang ZR, Thomson R, McNeil P, Esnouf RM (2005) RONN: the bio-basis function neural network technique applied to the detection of natively disordered regions in proteins. Bioinformatics **21:** 3369–3376

Zamyatnin AA Jr, Solovyev AG, Savenkov EI, Germundsson A, Sandgren M, Valkonen JPT, Morozov SY (2004) Transient coexpression of individual genes encoded by the triple gene block of potato mop-top virus reveals requirements for TGBp1 trafficking. Mol Plant Microbe Interact **17:** 921–930

Supplemental Data

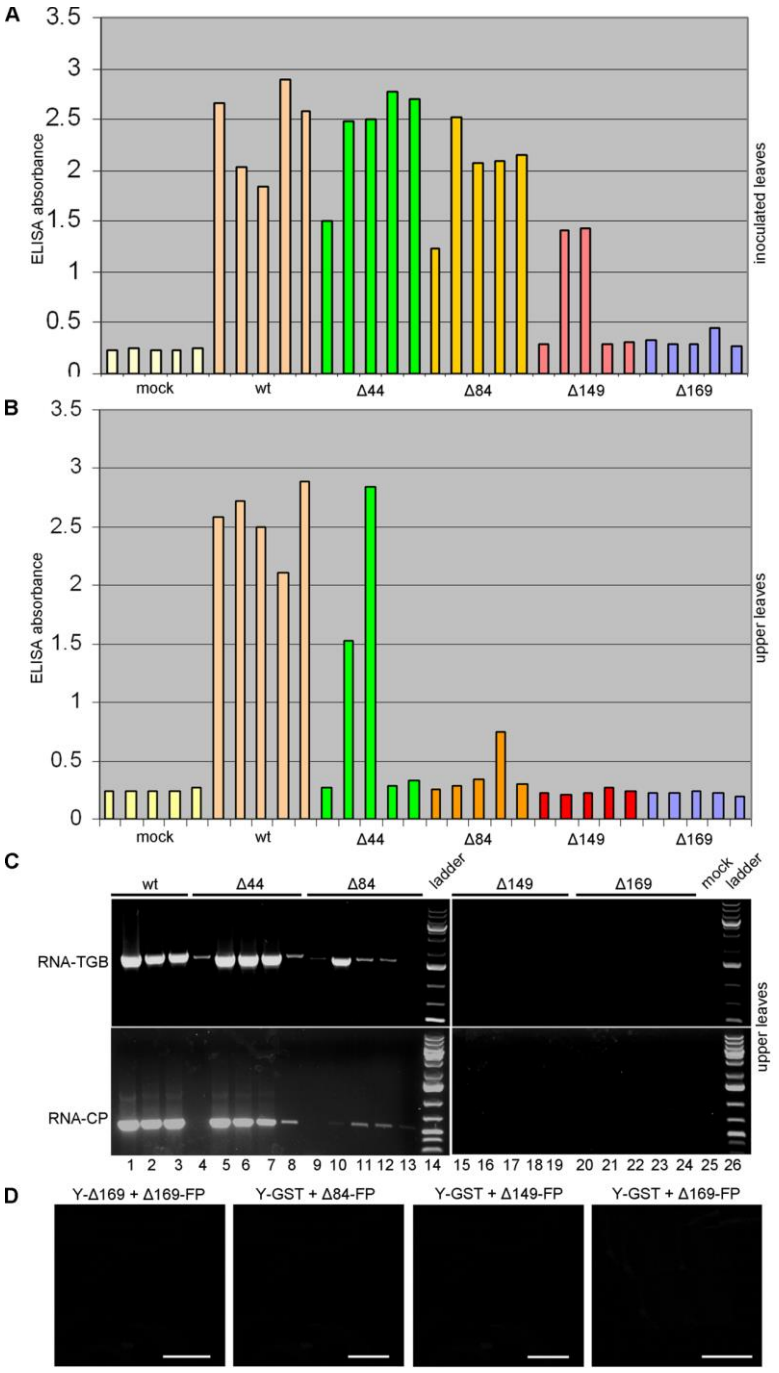

Figure S1. The effects of the 5'-proximal deletions in the TGB1 cistron on virus accumulation in inoculated and upper leaves and on interactions of the truncated TGB1 derivatives.
A, **B**, Levels of PMTV CP-antigen detected by ELISA as indicated by absorbance values at 405 nm. Plant extracts were prepared from inoculated leaves (A) and upper leaves (B) 14 dpi. The data are from the first experiment (n=5, five plants analysed for each treatment). **C**, RT-PCR detection of PMTV RNA-CP and RNA-TGB in *N. benthamiana* plants inoculated with *in vitro* transcripts of RNA-Rep, RNA-CP and RNA-TGB deletion mutants. At 14 dpi total RNA was extracted from upper non-inoculated leaves and used as template in RT-PCR amplification of RNA-TGB (upper panels) and RNA-CP (lower panels). In A-C, each bar in the charts and each lane in the RT-PCR gels represents an individual plant. **D**, The absence of self-interaction of Δ169 detected by BiFC assay and expression of Δ84-FP, Δ149-FP and Δ169-FP with Y-GST as negative controls for BiFC assays shown in Fig. 2D and 5A. Scale bar, 20 μm.

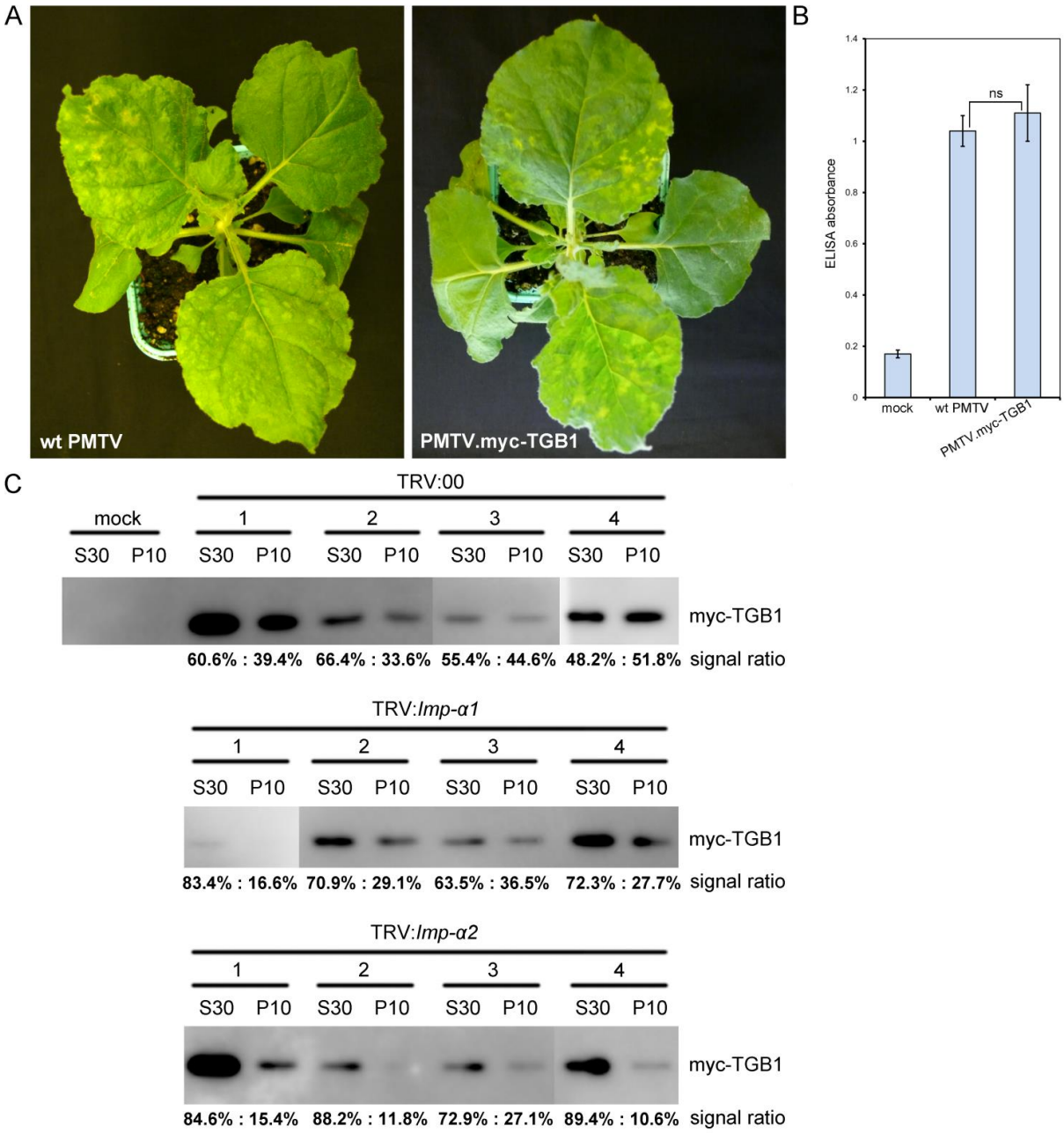

Figure S2. Characterisation of PMTV.myc-TGB1 construct.
A, Appearance of PMTV symptoms (yellow mosaic) in *N. benthamiana* infected with wt virus and PMTV.myc-TGB1 14 dpi. **B**, Accumulation of PMTV measured by ELISA as indicated by absorbance values at 405 nm. Plant extracts were prepared from upper leaves 14 dpi. The average absorbance of a healthy plant extract (m, mock) was equal to 0.18. ELISA experiments were conducted twice (n=6). The error bars denote SD; ns, not significant (P> 0.05, Student's t test). **C**, Presence of myc-tagged TGB1 in the nuclear P10 and cytoplasmic S30 fractions of the upper leaves of the plants infected with PMTV.myc-TGB1. The fractions were analyzed by immunoblotting using antisera to the myc-tag. Data (along with the data shown in Fig. 6E) are from two independent experiments and were used for quantification shown in Fig. 6F.

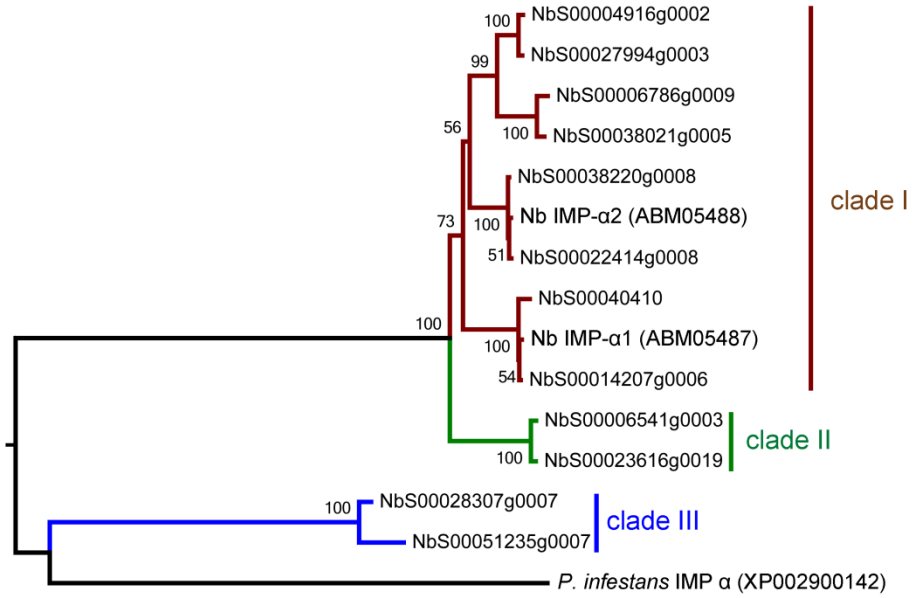

Figure S3. Phylodendrogram of the fourteen *N. benthamiana* importin-α isoforms.
Alignments were performed using ClustalW and the tree was prepared in MEGA6. *Phytophthora infestans* importin α was used as an outgroup. Numbers represent accessions from the Sol genomics database and GenBank accession numbers. Asterisks denote the importin α isoforms investigated in this study. Sequences used to generate the phylodendrogram are presented in Supplemental Data Set 1 online.

Supplemental Data Set 1 online.
Sequences used to generate phylodendrogram in Supplemental Figure S3.